Optical Tamm states in 2D nanostructured magnetophotonic structures

Baptiste Mathmann, Oumaima Haidar, Abdelkrim Talbi, Nicolas Tiercelin, Abdallah Mir, El Houssaine El Boudouti, Bahram Djafari-Rouhani, Gaëtan Lévêque, Abdellatif Akjouj, Yannick Dusch

Optical Tamm states in 2D nanostructured magnetophotonic structures

Baptiste Mathmann

baptiste.mathmann@centralelille.fr

Univ. Lille, CNRS, Centrale Lille, Univ. Polytechnique Hauts-de-France, UMR 8520-IEMN, F-59000 Lille, France

Oumaima Haidar

Univ. Lille, CNRS, Centrale Lille, Univ. Polytechnique Hauts-de-France, UMR 8520-IEMN, F-59000 Lille, France

Abdelkrim Talbi

Univ. Lille, CNRS, Centrale Lille, Univ. Polytechnique Hauts-de-France, UMR 8520-IEMN, F-59000 Lille, France

Nicolas Tiercelin

Univ. Lille, CNRS, Centrale Lille, Univ. Polytechnique Hauts-de-France, UMR 8520-IEMN, F-59000 Lille, France

Abdallah Mir

Laboratory of Advanced Materials Studies and Applications (LEM2A), Physics Department, Faculty of Science, Moulay Ismail University of Meknes, B.P.11201 Zitoune Meknes, Morocco

El Houssaine El Boudouti

LPMR, Département de Physique, Faculté des Sciences, Université Mohammed I, 60000 Oujda, Morocco

Bahram Djafari Rouhani

Univ. Lille, CNRS, Centrale Lille, Univ. Polytechnique Hauts-de-France, UMR 8520-IEMN, F-59000 Lille, France

Gaëtan Lévêque

Univ. Lille, CNRS, Centrale Lille, Univ. Polytechnique Hauts-de-France, UMR 8520-IEMN, F-59000 Lille, France

Abdellatif Akjouj

Univ. Lille, CNRS, Centrale Lille, Univ. Polytechnique Hauts-de-France, UMR 8520-IEMN, F-59000 Lille, France

Yannick Dusch

Univ. Lille, CNRS, Centrale Lille, Univ. Polytechnique Hauts-de-France, UMR 8520-IEMN, F-59000 Lille, France

Research Article

Keywords: Magnetoplasmonics, MOKE, Tamm plasmon, Nanostructures

Posted Date: February 23rd, 2024

DOI: https://doi.org/10.21203/rs.3.rs-3972508/v1

Additional Declarations: No competing interests reported.

Optical Tamm states in 2D nanostructured magnetophotonic structures

Baptiste Mathmann[1*], Oumaima Haidar[1,2], Abdelkrim Talbi[1], Nicolas Tiercelin[1], Abdallah Mir[2], El Houssaine El Boudouti[3], Bahram Djafari Rouhani[1], Gaëtan Lévêque[1], Abdellatif Akjouj[1], Yannick Dusch[1]

[1]Univ. Lille, CNRS, Centrale Lille, Univ. Polytechnique Hauts-de-France, UMR 8520-IEMN, F-59000 Lille, France.
[2]Laboratory of Advanced Materials Studies and Applications (LEM2A), Physics Department, Faculty of Science, Moulay Ismail University of Meknes, B.P.11201 Zitoune Meknes, Morocco.
[3]LPMR, Département de Physique, Faculté des Sciences, Université Mohammed I, 60000 Oujda, Morocco.

Abstract

We numerically explore optical Tamm states (OTS) supported by a photonic structure composed of a nanostructured metallic layer on top of a distributed Bragg reflector (DBR). Several polarizations, incidences and patterning are assessed to map OTS and their properties. We then gain magnetic control of the OTS by adding a cobalt layer below the metal pattern and switching its magnetization. This control, widely used in plasmonics, takes advantage of the Transverse Magneto-Optical Kerr Effect (TMOKE). The simulated TMOKE signal of this structure has an amplitude of the order of 10^{-3} and, compared to conventional magnetoplasmonic structures, provides high energy confinement between the metal stripes. In addition to the opening of the metallic layer that allows better access of the analyte to the sensitive area, this paves the way for higher sensitivities in bio- and chemical sensing applications.

Keywords: Magnetoplasmonics, MOKE, Tamm plasmon, Nanostructures

1 Introduction

Optical Tamm states (OTS), are highly confined electromagnetic states appearing at the interface between a Bragg mirror, also called distributed Bragg reflector (DBR), and a medium with negative dielectric constant [1]. OTS are remarkable for the narrow width of their resonance, usually in the 10 nm range, as well as for the confinement of the electromagnetic energy which decreases exponentially from the surface [2]. OTS can also be referred to as Tamm plasmons if a plasmonic material is used due to their similarities with surface plasmon polariton (SPP). However OTS have several advantages over SPP. OTS can be excited in both TE and TM polarization whereas SPP needs TM polarization to be excited. They can also be excited directly without the need for a prism or a grating since, contrary to the SPP, their dispersion curve lies above the light line [3].

Since their first theoretical prediction [2] and experimental observation [4], OTS have been studied over several years for their wide variety of possible interactions with other modes such as SPP [5], cavity mode [6] or bound state in the continuum [7]. Several ways to tune and control OTS have also been investigated, among them one can cite liquid crystals [8], the pattering of the metallic surface [9] or the addition of a magnetic layer [10]. Due to their qualities and versatility, OTS have been considered for many applications such as sensing [11], optical control [12] or lasing [13].

We propose to take advantage of the peculiar features of OTS to provide Transverse Magneto-Optical Kerr Effect (TMOKE) signals in 2D magnetophotonic structures, in which energy confinement at and below the air/dielectric interface can be obtained.

2 Model

The general structure used to excite OTS is shown on Fig. 1. It is composed of a DBR with a 2D array of gold nanostripes. The materials chosen for the DBR are silicon nitride (Si_3N_4) and silicon dioxide (SiO_2). Their refractive indexes are taken from Luke *et al.* [14] and Maltison [15] respectively. The materials and number of bilayers of the DBR are chosen according to experimental constraints for a later fabrication of the device using plasma enhanced chemical vapor deposition (PECVD) for the DBR and e-beam lithography for the gold nanostripes. In this paper, we use simulations to explore the best results that could be demonstrated in a future experimental investigation. The technological constraints also dictate our choice of working wavelength of 800 nm - 1200 nm as smaller wavelength implies too small nanostripes width while larger wavelength requires thicker DBR which are difficult to fabricate. For the simulations, the structure is considered to have a periodic array of nanostripes of infinite length. This is numerically implemented using Floquet boundary conditions. The structure is deposited on a SiO_2 substrate where perfectly matched layers are added to prevent reflection. The numerical studies have been done using the commercial finite element method software COMSOL Multiphysics.

We explore different 1D patterning, either symmetric (simple period) or asymmetric (double period), with different planes of incidence (POI) and polarization (see Fig. 1). The illumination is done in free space from the metallic layer side. OTS obtained for an unpatterned metallic layer is studied for reference.

As common in magnetoplasmonics, we then introduce a thin cobalt layer underneath the gold layer. Cobalt is considered to be isotropic and magnetized along the x-axis with a permittivity tensor given by [16]:

$$\bar{\varepsilon} = \varepsilon_0 N^2 \begin{bmatrix} 1 & 0 & 0 \\ 0 & 1 & iQ \\ 0 & -iQ & 1 \end{bmatrix}, \tag{1}$$

where $N = n + ik$ is the complex refractive index of the cobalt and Q its magneto-optic constant taken equal to $Q = 0.0212 - 0.007i$ at saturation magnetization [17]. Q being linear in magnetization M, we consider $Q(+M) = -Q(-M)$. Several configurations, including TMOKE, LMOKE and PMOKE (for transverse, longitudinal and polar magneto optical Kerr effect respectively), in either TE or TM polarization, with varying angles of incidence have been numerically assessed. As expected from the symmetries of the magneto-optical effect, only TMOKE with TM polarization and a non-zero angle of incidence provides a magnetic differential response when switching magnetization direction from $+M$ to $-M$.

3 Results and discussion

3.1 OTS in 2D photonic crystal

It is known that an unpatterned metallic layer on a DBR can support OTS. Since this structure is 1D along the z axis, the electric field at the resonance only depends on the z coordinate with an homogeneous distribution of the energy in x and y directions. These modes will be referred to as conventional Tamm modes. The opening of the metallic layer is interesting for sensing applications as it allows for an analyte to penetrate deeper in the device toward the zone of highest energy density, improving sensitivity. Additionally, if the opening is done with a pattern and the right configuration, modes other than the conventional Tamm mode can be excited. We consider four different configurations : TE or TM polarization, both with the projection of the electric field in the Oxy-plane parallel or perpendicular to the stripes (see Fig. 1(a) and Table 1). As shown on Fig. 2, a schematic dispersion diagram of the excited modes for each configuration can be obtained by superposition of the curves extracted from the dispersion diagram that were calculated for all configurations. The wave vector k represent either kx or ky depending on the POI as illustrated in Fig. 1 (a).

For the simple period design, all configurations only support conventional Tamm modes except for TE with an electric field parallel to the stripes. The effect of nanostructuration is only to produce a shift in the resonance while keeping the parabolic shape of the dispersion curve. As seen in Fig. 2, if the electric field direction is parallel to the stripes, there is a shift of the resonance towards longer wavelengths compared to the same resonance on an unpatterned device. Otherwise, if the electric field is perpendicular, the resonance is shifted towards shorter wavelengths.

Among all the configurations, the one with a TE polarization and the electric field parallel to the stripes was shown by Ferrier *et al.* to allow for the excitation of other interesting modes [18]. They are created by a symmetry break (Figs. 1(b)) that leads to a bandgap opening at the end of the Brillouin zone (Fig. 2). The lower frequency mode

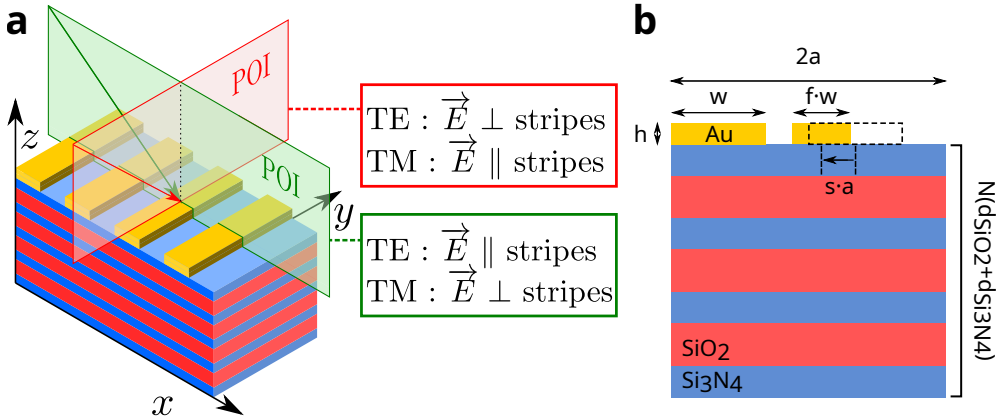

Fig. 1 (a) The different studied configurations and how the choice of the POI and polarization determines the orientation of the electric field relative to the stripes. (b) Schematic of the double period structure. The dashed stripe represents the simple period structure before the stripe was shrinked by a factor f and shifted by a factor s.

is called the air mode because the energy is concentrated just below the air between the stripes. The higher frequency one is called the metal mode for the energy is concentrated below the metal stripes. This concentration of the electromagnetic energy is illustrated in Fig. 3(b). The air mode is especially interesting for sensing applications as the energy is further concentrated between the stripes where an analyte can penetrate. Using a porous material would allow the analyte to reach the region of highest energy density in the last layer between the stripes, taking better advantage of the concentration of the energy. A drawback is that these modes require an important angle of incidence to be excited and can even be below the light line. However, by breaking the pattern symmetry they can be made accessible for reflectivity measurements in free space, thus providing an access for analytes in sensing applications. It is done by implementing a double period pattern with one of the gold stripes shrunken and shifted [18]. The general geometry for such a device is represented in Fig. 1(b). Hence, in the case of double period and electric field parallel to the stripes in TE, one can find the same modes as in the simple period case but now folded in a reduced Brillouin zone. Note that the shifting and shrinking of every two stripes doesn't allow air and metal mode excitation when the electric field is perpendicular to the stripes.

It is interesting to remark that the simple period patterning in the TM polarization only shifts the resonance without bandgap opening or folding like in TE. Additionally, since TE and TM dispersion diagrams intersect at normal incidence, the symmetry breaking of the double period design allows the air and metal modes to be excited at normal incidence and for TM polarization as well. Their dispersion curves in TM appear to be parabolic like in the conventional mode. Hence they have a different shape of dispersion curve in TE and in TM.

We choose the configuration with TE polarization and the electric field parallel to the stripes with the double period design to take advantage of the high energy confinement and the possibility to do measurements in free air at normal incidence. Such a structure has been optimized to provide two high quality factor resonances

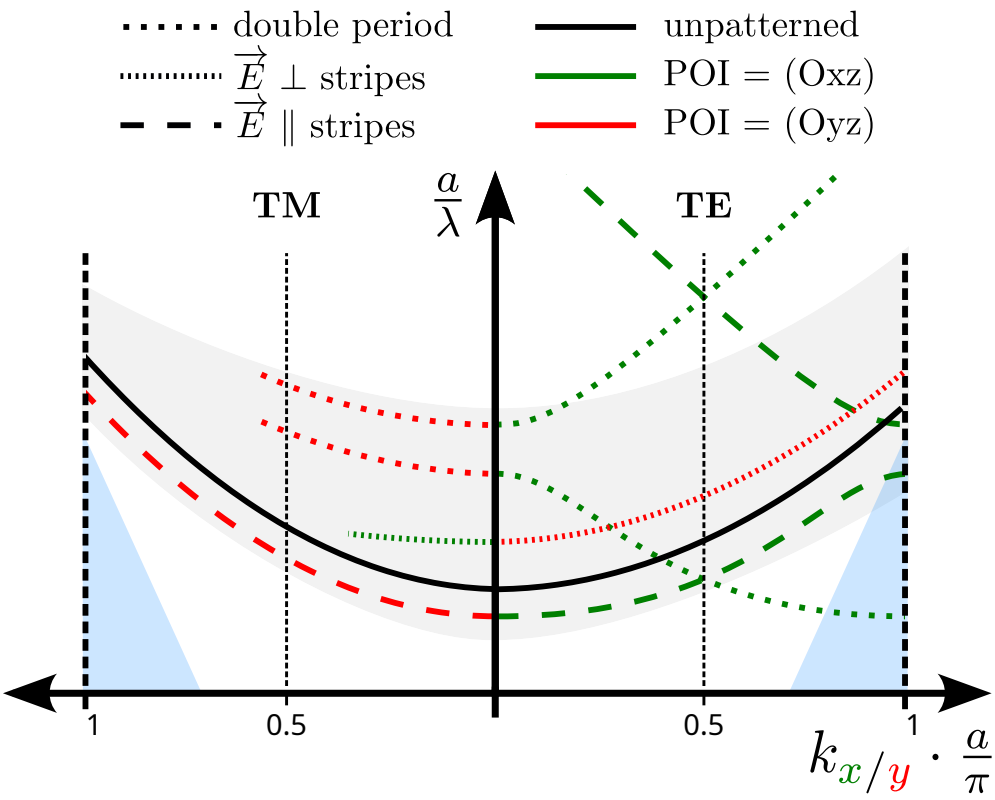

Fig. 2 Schematic dispersion diagram of different resonances that can be excited in a Tamm structure depending on the patterning, polarization and plane of incidence. a is related to he pattern period and defined in Fig. 1. The unpatterned device is shown in black for reference. The greyed area represents the DBR bandgap and the blue one the zone below the free air light line.

in the near-infrared range. Enhancement of the Tamm mode resonance is expected at the very edge of the DBR [13]. Thus, the thickness of the last layer of the DBR is a relevant parameter as its modification allows for a tailoring of the resonance wavelength by changing the phase matching condition. It can be used to choose a specific wavelength for the resonance or improve its quality factor as well as increase the energy confinement in the vicinity of the surface [19]. This thickness variation of the last layer will be called Δ.

The optimization goal is to have good quality factors for air and metal modes at normal incidence. A sweep of each of the parameters listed below guarantee a local maximum (see Fig. 1 for the definition of the geometrical parameters). It led to the following values :

- a = 460 nm : system periodicity
- w = 250 nm : width of a basic gold stripe
- f = 0.55 : scaling factor of the first design
- s = 0.1 : shifting factor of the first design

- h = 100 nm : gold thickness
- N = 10 : number of bilayers of the DBR
- d_{SiO_2} = 181 nm : SiO_2 thickness
- $d_{Si_3N_4}$ = 130 nm : Si_3N_4 thickness
- Δ = 0 nm : thickness variation for the last SiN layer

The simulated energy-momentum dispersion diagram in free space for a TE polarization and wave vector perpendicular to the stripes is presented in Fig. 3(c). As expected, two distinct peaks at 939 (metal mode) and 984 nm (air mode) create a bandgap at the edge of the spectral window created by the DBR. Their quality factor are 275 and 271 respectively. The ripples in the OTS dispersion diagram comes from the interaction of OTS and the folding of the DBR oscillations [9].

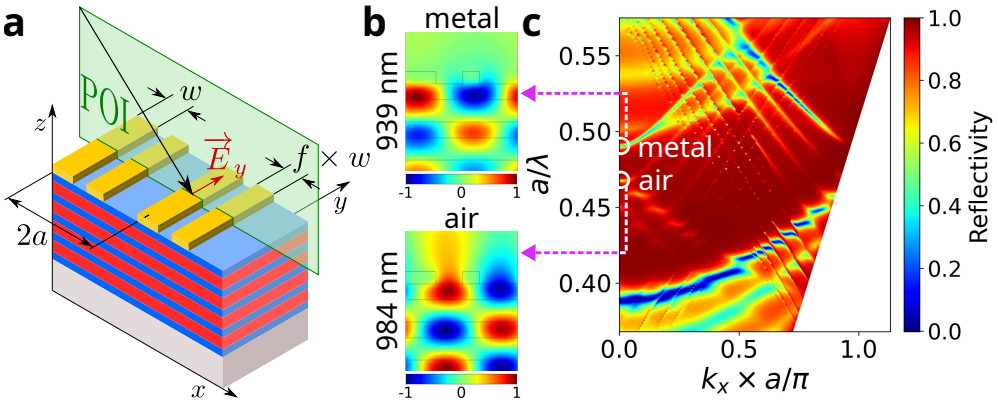

Fig. 3 (a) Schematic view of the double period structure with the TE incident wave. (b) Distribution of the out-of-plane electric field, for both the metal mode and the air mode. (c) Energy-momentum dispersion diagram of the structure obtained from reflectivity (color scale).

3.2 OTS in 2D magnetophotonic structure

The spectral position of a Tamm state can be controlled by changing the magnetization of a magneto-optical layer positioned between the metallic layer and the DBR [20]. This can be used to enhance the magneto-optical Kerr effect and create a sensing device similar to already existing magneto-plasmonic sensors [21].

The TMOKE signal can be highlighted only in TM polarization. For the simple period design, both configurations (with the electric field parallel or perpendicular to the stripes) allow a TMOKE signal on a conventional Tamm mode [10]. However, for the double period design, we want to take advantage of the higher energy concentration of the air and metal modes that only appear when the electric field is parallel to the stripes. Hence, an electric field parallel to the stripes and a TM polarization is the most interesting configuration as it is the only one that allows TMOKE signal for the air and metal modes (Table 1).

Table 1 Excitable modes and magnetic signal for the different configurations.

	$\vec{E} \parallel$ stripes	$\vec{E} \perp$ stripes
TE	Air & metal	-
TM	Air & metal, TMOKE	TMOKE

In Fig. 4, we calculate the dispersion diagram for the double period design in TM polarization, compare it with the one for the simple period (same parameters except s=0 and f=1) and then look at both reflectivity and TMOKE signal. The design is the same as in Fig. 3 with the addition of a 6 nm thick cobalt layer below the gold to allow for a magnetic effect. The POI and polarization have also been both changed to allow for a TMOKE signal and the air and metal modes excitation. The TMOKE response is defined as follows:

$$TMOKE = \frac{R(+M) - R(-M)}{R(+M) + R(-M)} \ , \tag{2}$$

where $R(+M)$ and $R(-M)$ are the reflectivities with a magnetisation in the x and $-x$ direction, respectively.

Comparing Fig. 4(a) and (c) shows that the symmetry break only adds new modes in TM but without folding as well as the parabolic shape of said modes. Conventional mode and the apparition of the air and metal modes ($a/\lambda = 0.45$ and 0.47 at normal incidence respectively) in the double period design are clearly visible and, if the TMOKE signal is stronger for the conventional one by an order of magnitude, a TMOKE signal is present for the air and metal ones. It is possible to increase the TMOKE signal for the air or metal modes by changing the geometry. Here we give the example of a design oriented towards TMOKE signal for the air mode.

Optimization is done the same way as previously, with a sweep of each parameter to ensure a local maximum. The amplitude of the TMOKE signal is found to be the highest at 15°. For the thickness of the cobalt layer, a compromise had to be found as a thicker layer decreases the quality of the resonance due to high ohmic losses while increasing the magnetization effects and thus the TMOKE signal. Best results are found for a cobalt thickness of 6 nm. The other parameters are chosen as follows :

- a = 400 nm : system periodicity
- w = 210 nm : width of a gold stripe
- f = 0.45 : scaling factor
- s = 0.3 : shifting factor
- h = 54 nm : gold thickness
- N = 6 : number of bilayers of the DBR
- d_{SiO_2} = 181 nm : SiO_2 thickness
- $d_{Si_3N_4}$ = 130 nm : Si_3N_4 thickness
- Δ = -30 nm : thickness variation for the last Si_3N_4 layer

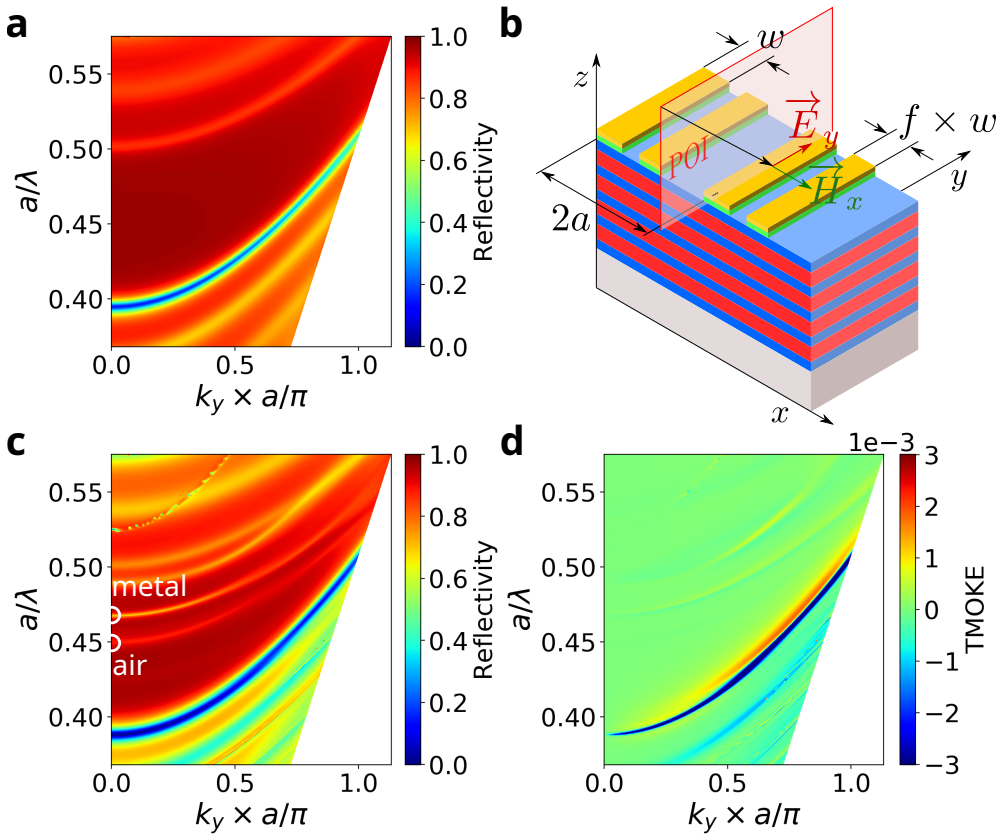

Fig. 4 (a) Dispersion diagram from reflectivity of the simple period structure in TM polarization. (b) Schematic view of the structure with the TM incident wave. (c) Reflectivity and (d) TMOKE response of the double period structure in TM polarization.

The dispersion diagram from reflectivity, presented in Fig. 5(a), shows a metal mode, a much strongly peaked air mode and no conventional mode. Here the conventional OTS is no longer excitable as the changes in the geometry push it out of the Bragg mirror's bandgap. The corresponding TMOKE signal in Fig. 5(b) confirms that the obtained signal is stronger for the air mode.

As shown in Fig. 5(c), the spectral response of the structure at 15° incidence exhibits a strongly peaked resonance at 902 nm which corresponds to an air mode, as indicated by the localization of the electric field visible in the insert. The metal mode, while less peaked, is still noticeable at 856 nm. The air and metal modes have a quality factor of 37 and 42 respectively. The decrease in quality factor is due to losses in the cobalt. The localization of the electric field also indicate that air and metal modes in TM keep their localization of the energy below or between the stripes for any angle of incidence while in TE it is only true at the center and the end of the Brillouin zone ($k_x\ a/\pi = 0$ or 1).

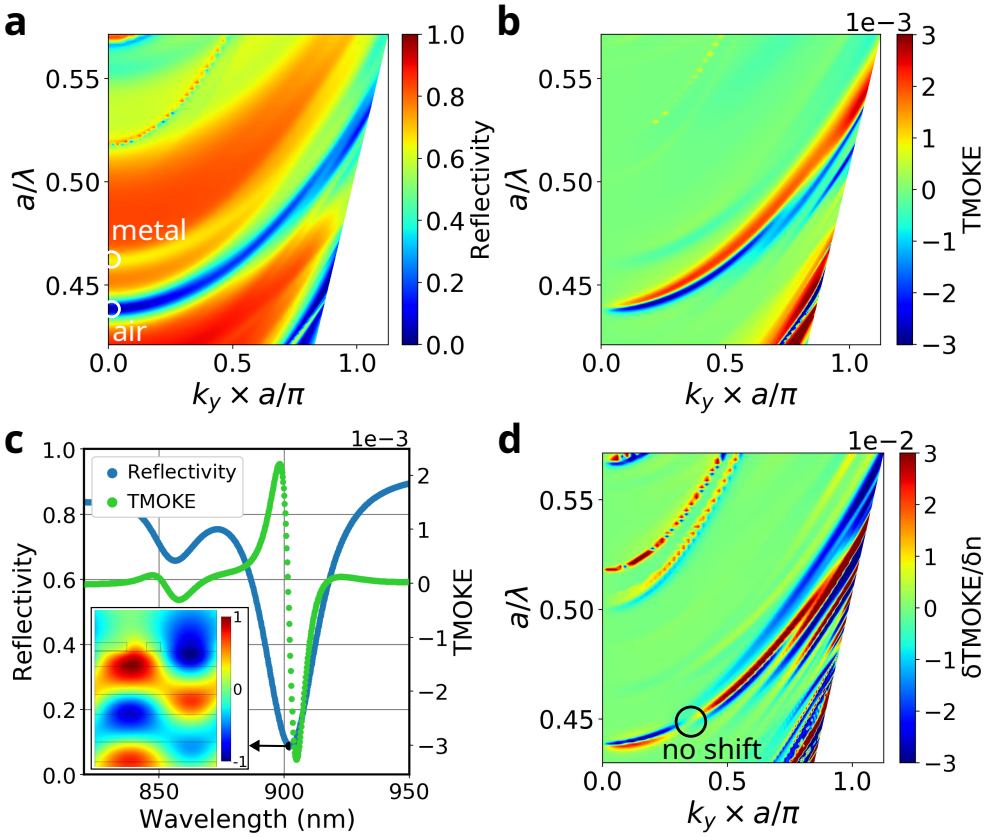

Fig. 5 (a) Reflectivity and (b) TMOKE signal of the double period device with the gold and cobalt bilayer nanostripes. (c) Cut of top dispersion diagrams for an angle of incidence of 15°. The inset represents the distribution of the out-of-plane electric field at the air resonance (902 nm). (d) Difference in the magnetic signal relative to the change in refractive index for an index of 1.0001 and a reference index of 1

The amplitude of the TMOKE signal is of the order of 10^{-3} for the air mode, which corresponds to typical values obtained in magnetoplasmonic devices [22]. The TMOKE signal for the metal mode, which wasn't the focus here, while smaller by an order of magnitude, is still noticeable.

Now that we have obtained a magnetic signal for an air mode, it must be checked if this signal is sensitive to refractive index changes of the analyte. As a test, we ran simulations with a refractive index of the analyte of 1.01, 1.001, 1.0001 and compared them to a reference with a refractive index of 1. It must be noted that this device hasn't been optimised for sensitivity. A change in the thickness of the last layer of the DBR could increase the confinement of the energy close to the surface and improve the sensitivity. The change in TMOKE amplitude relative to the change in refractive index $\delta TMOKE/\delta n$ is found to be equal for the tested indexes. The result for n =

1.0001, which correspond to typical index variations in plasmonic sensing characterisation [23, 24], is shown in Fig. 5(d). It shows a shift of the TMOKE signal when the refractive index increases. This shift occurs in opposite directions depending on the angle of incidence with an angle where no shift happens at around 23°. This drop in sensitivity at a certain angle must be kept in mind if this device is to be used for sensing applications.

4 Conclusion

We have numerically observed the excitable OTS in a 2D photonic structure. In these structures, the energy of the incident electromagnetic wave is strongly confined in the vicinity of the surface (owing to the nature of OTS), and between the metallic stripes (owing to the surface nanostructuration). Additionally, the nanostructuration allows for an opening of the metallic layer and provides an access for the analyte to the region of high energy density. We showed that some configurations in TM polarization provides supplementary features such as a stability of the energy confinement when varying the angle of incidence and the possibility to observe a TMOKE signal. Further study showed a TMOKE signal of the order of 10^{-3}, which is comparable to values obtained in magnetoplasmonics structures, as well as a sensitivity of the TMOKE signal to refractive index variations. This paves the way for high sensitivity bio- and chemical sensors using surface functionalization. Further work will include experimental study of the proposed structure as well as a thorough evaluation of the sensing potential of this device.

Statements and Declarations

Funding. This work was supported by Conseil Régional Hauts-de-France (Hauts-de-France Regional Council) and Centrale Lille Institut.

Competing Interests. The authors declare no competing interests.

Author Contributions. **Baptiste Mathmann**: Conceptualization (equal); Formal analysis (equal); Investigation (equal); Methodology (equal); Visualization (equal); Writing - original draft (equal); Writing – review & editing (equal) **Oumaima Haidar**: Validation (equal); Writing – review & editing (equal) **Abdelkrim Talbi**: Conceptualization (equal); Formal analysis (equal); Funding acquisition (equal); Methodology (equal); Supervision (equal); Writing – review & editing (equal) **Nicolas Tiercelin**: Funding acquisition (equal); Supervision (equal); Writing – review & editing (equal) **Abdallah Mir**: Funding acquisition (equal); Supervision (equal) **El Houssaine El Boudouti**: Writing – review & editing (equal) **Bahram Djafari Rouhani**: Writing – review & editing (equal) **Gaëtan Lévêque**: Supervision (equal) **Abdellatif Akjouj**: Supervision (equal) **Yannick Dusch**: Conceptualization (equal); Formal analysis (equal); Funding acquisition (equal); Methodology (equal); Supervision (equal); Visualization (supporting); Writing – review & editing (equal)

Data Availability. The datasets generated during and analyzed during the current study are available from the corresponding author on reasonable request.

References

[1] Kaliteevski, M., Iorsh, I., Brand, S., Abram, R., Chamberlain, J., Kavokin, A., Shelykh, I.: Tamm plasmon-polaritons: Possible electromagnetic states at the interface of a metal and a dielectric bragg mirror. Physical Review B **76**(16), 165415 (2007)

[2] Kavokin, A., Shelykh, I., Malpuech, G.: Lossless interface modes at the boundary between two periodic dielectric structures. Physical Review B **72**(23), 233102 (2005)

[3] Kar, C., Jena, S., Udupa, D.V., Rao, K.D.: Tamm plasmon polariton in planar structures: A brief overview and applications. Optics & Laser Technology **159**, 108928 (2023)

[4] Sasin, M., Seisyan, R., Kalitteevski, M., Brand, S., Abram, R., Chamberlain, J., Egorov, A.Y., Vasil'Ev, A., Mikhrin, V., Kavokin, A.: Tamm plasmon polaritons: Slow and spatially compact light. Applied Physics Letters **92**(25), 251112 (2008)

[5] Chen, Y., Zhang, D., Zhu, L., Fu, Q., Wang, R., Wang, P., Ming, H., Badugu, R., Lakowicz, J.R.: Effect of metal film thickness on tamm plasmon-coupled emission. Physical Chemistry Chemical Physics **16**(46), 25523–25530 (2014)

[6] Lu, H., Li, Y., Jiao, H., Li, Z., Mao, D., Zhao, J.: Induced reflection in tamm plasmon systems. Optics Express **27**(4), 5383–5392 (2019)

[7] Bikbaev, R.G., Maksimov, D.N., Pankin, P.S., Chen, K.-P., Timofeev, I.V.: Critical coupling vortex with grating-induced high q-factor optical tamm states. Optics Express **29**(3), 4672–4680 (2021)

[8] Buchnev, O., Belosludtsev, A., Reshetnyak, V., Evans, D.R., Fedotov, V.A.: Observing and controlling a tamm plasmon at the interface with a metasurface. Nanophotonics **9**(4), 897–903 (2020)

[9] Qiao, T., Hu, M., Jiang, X., Wang, Q., Zhu, S., Liu, H.: Generation and tunability of supermodes in tamm plasmon topological superlattices. ACS Photonics **8**(7), 2095–2102 (2021)

[10] Dong, H.Y., Wang, J., Cui, T.J.: One-way tamm plasmon polaritons at the interface between magnetophotonic crystals and conducting metal oxides. Physical Review B **87**(4), 045406 (2013)

[11] Auguié, B., Fuertes, M.C., Angelomé, P.C., Abdala, N.L., Soler Illia, G.J., Fainstein, A.: Tamm plasmon resonance in mesoporous multilayers: toward a sensing application. ACS Photonics **1**(9), 775–780 (2014)

[12] Gazzano, O., De Vasconcellos, S.M., Gauthron, K., Symonds, C., Bloch, J., Voisin, P., Bellessa, J., Lemaître, A., Senellart, P.: Evidence for confined tamm plasmon

modes under metallic microdisks and application to the control of spontaneous optical emission. Physical Review Letters **107**(24), 247402 (2011)

[13] Lheureux, G.: Étude de l'effet laser dans les structures à plasmon tamm. PhD thesis, Lyon 1 (2015)

[14] Luke, K., Okawachi, Y., Lamont, M.R., Gaeta, A.L., Lipson, M.: Broadband mid-infrared frequency comb generation in a si 3 n 4 microresonator. Optics Letters **40**(21), 4823–4826 (2015)

[15] Malitson, I.H.: Interspecimen comparison of the refractive index of fused silica. J. Opt. Soc. Am. **55**(10), 1205–1209 (1965)

[16] Qiu, Z., Bader, S.D.: Surface magneto-optic kerr effect (smoke). Journal of Magnetism and Magnetic Materials **200**(1-3), 664–678 (1999)

[17] Dehesa-Martínez, C., Blanco-Gutierrez, L., Vélez, M., Diaz, J., Alvarez-Prado, L., Alameda, J.: Magneto-optical transverse kerr effect in multilayers. Physical Review B **64**(2), 024417 (2001)

[18] Ferrier, L., Nguyen, H.S., Jamois, C., Berguiga, L., Symonds, C., Bellessa, J., Benyattou, T.: Tamm plasmon photonic crystals: From bandgap engineering to defect cavity. APL Photonics **4**(10), 106101 (2019)

[19] Symonds, C., Azzini, S., Lheureux, G., Piednoir, A., Benoit, J.-M., Lemaitre, A., Senellart, P., Bellessa, J.: High quality factor confined tamm modes. Scientific Reports **7**(1), 3859 (2017)

[20] Fang, Y.-t., Ni, Y.-x., He, H.-q., Hu, J.-x.: Effect of hybrid state of surface plasmon–polaritons, magnetic defect mode and optical tamm state on nonreciprocal propagation. Optics Communications **320**, 99–104 (2014)

[21] Wu, J., Yang, X., Wang, Z., Wu, B., Wu, X.: Giant enhancement of the transverse magneto-optical kerr effect based on the tamm plasmon polaritons and its application in sensing. Optics & Laser Technology **154**, 108353 (2022)

[22] Manera, M.G., Montagna, G., Ferreiro-Vila, E., González-García, L., Sánchez-Valencia, J., González-Elipe, A.R., Cebollada, A., Garcia-Martin, J.M., García-Martín, A., Armelles, G., *et al.*: Enhanced gas sensing performance of tio 2 functionalized magneto-optical spr sensors. Journal of Materials Chemistry **21**(40), 16049–16056 (2011)

[23] Ignatyeva, D.O., Knyazev, G.A., Kapralov, P.O., Dietler, G., Sekatskii, S.K., Belotelov, V.I.: Magneto-optical plasmonic heterostructure with ultranarrow resonance for sensing applications. Scientific reports **6**(1), 28077 (2016)

[24] Allsop, T., Neal, R., Davies, E.M., Mou, C., Bond, P., Rehman, S., Kalli, K.,

Webb, D.J., Calverhouse, P., Bennion, I.: Low refractive index gas sensing using a surface plasmon resonance fibre device. Measurement Science and Technology **21**(9), 094029 (2010)